Supporting Information

Engineering a Red Emission of Copper Nanoclusters Self-Assembly Architectures by Employing Aromatic Thiols as the Capping Ligands

Lin Ai,‡[a] Wanrun Jiang,‡[b] Zhaoyu Liu,[a] Jiale Liu,[a] Yang Gao,[b] Haoyang Zou,[a] Zhennan Wu,[a] Zhigang Wang,[b] Yi Liu,[a] Hao Zhang,[a,c] and Bai Yang[a]*

[a]State Key Laboratory of Supramolecular Structure and Materials, College of Chemistry, Jilin University, Changchun 130012, P. R. China.

[b]Institute of Atomic and Molecular Physics, Jilin University, Changchun 130012, P. R. China.

[c]Nanjing Haiyan Electric Technology Co. Ltd., Nanjing 211500, P. R. China.

‡These authors contributed equally.

*Address correspondence to hao_zhang@jlu.edu.cn

Figure S1. Low (a, b) and high (c, d) magnification TEM images of the self-assembly architectures composed of Cu NCs capped by 4-methylbenzenethiol (a, c) and 4-methoxybenzenethiol (b, d). Insets in (a, b): chemical structures of the capping ligands. Insets in (c, d): TEM size distribution of Cu NCs.

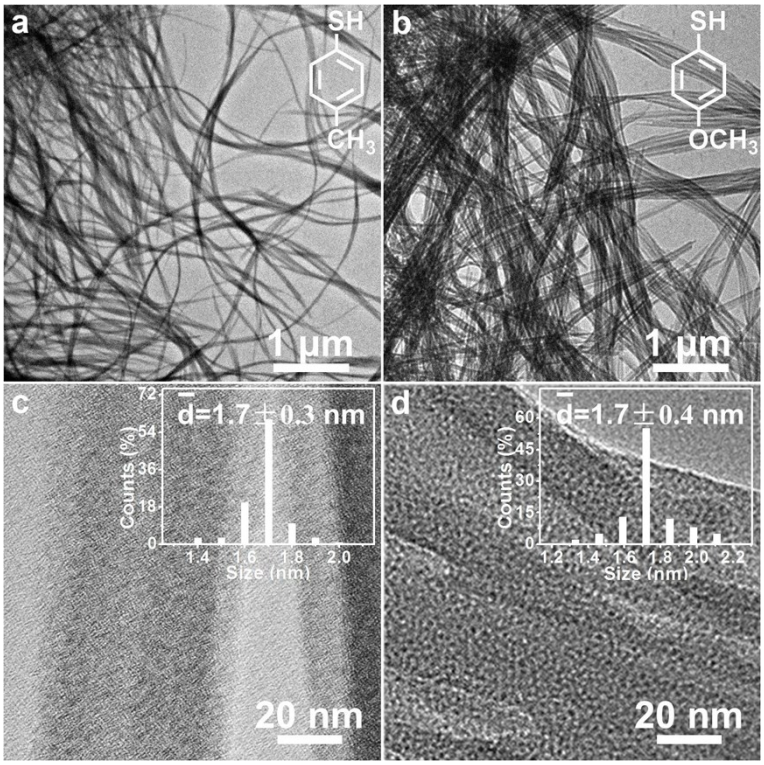

Figure S2. Low (a) and high (b) magnification TEM images of the NPs capped by 4-nitrothiophenol. Insets in (a): chemical structures of the capping ligands. Insets in (b): TEM size distribution of the NPs. (c) XPS Cu 2p spectrum of the NPs. The peaks at 951.9 and 932.3 eV are assigned to the Cu $2p_{1/2}$ and Cu $2p_{3/2}$ of Cu(0) or Cu(I). No characteristic satellite peak around 942 eV is observed, which implies the absence of Cu^{2+} in the NPs. (d) XRD pattern of the NPs, which indicates the composition of Cu_2S.

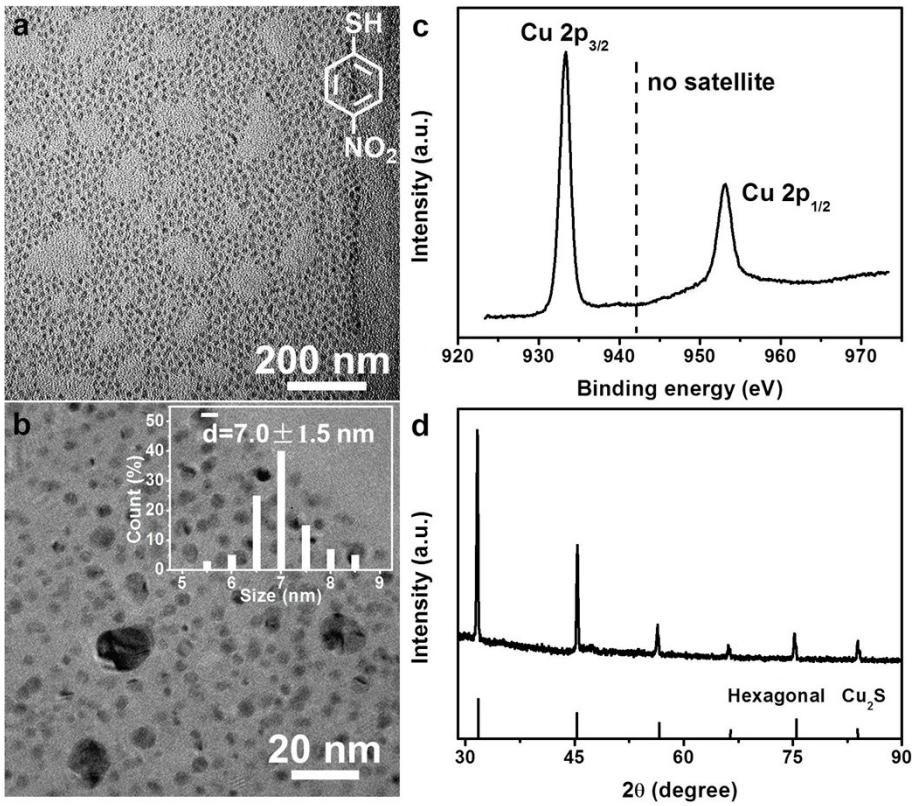

Figure S3. MALDI-TOF mass spectra (a-e) and EDX composition analysis (f-j) of the Cu NCs self-assembly architectures. L represents for the capping ligands in MALDI-TOF analysis peaks. The Mo signals in EDX result from the TEM Mo grid. The chemical structures of capping ligands are shown between MALDI-TOF data and EDX data.

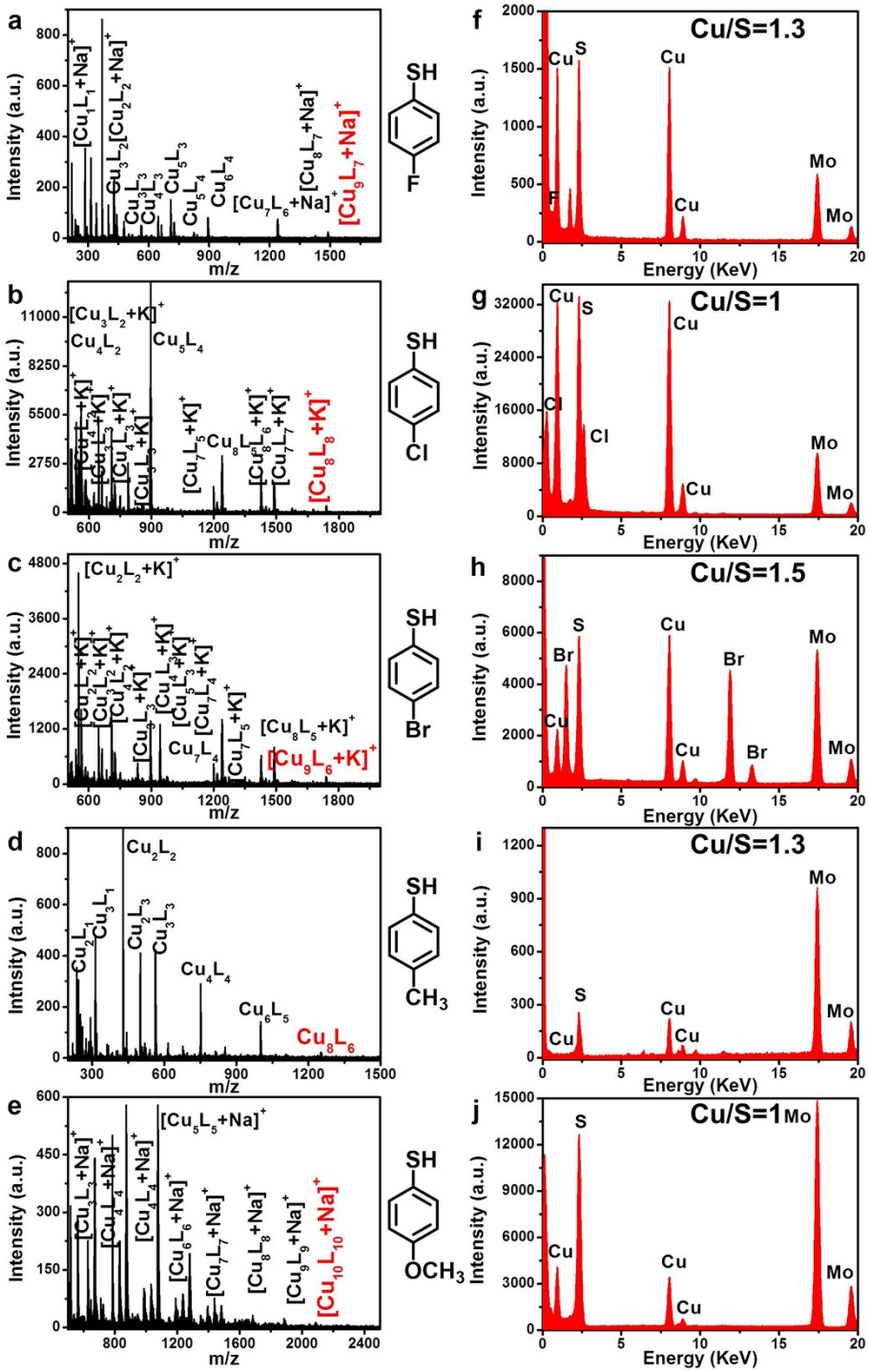

Figure S4. XPS spectra (a) and Cu LMM XAES spectra (b) of the Cu NCs self-assembly architectures. Cu LMM XAES spectra indicate the Cu(I)/Cu(0) molar ratio of 1/0, 3/1, 2/1, 1/0, and 3.5/1, respectively, for the ligands with increasing degree of electron-donating.

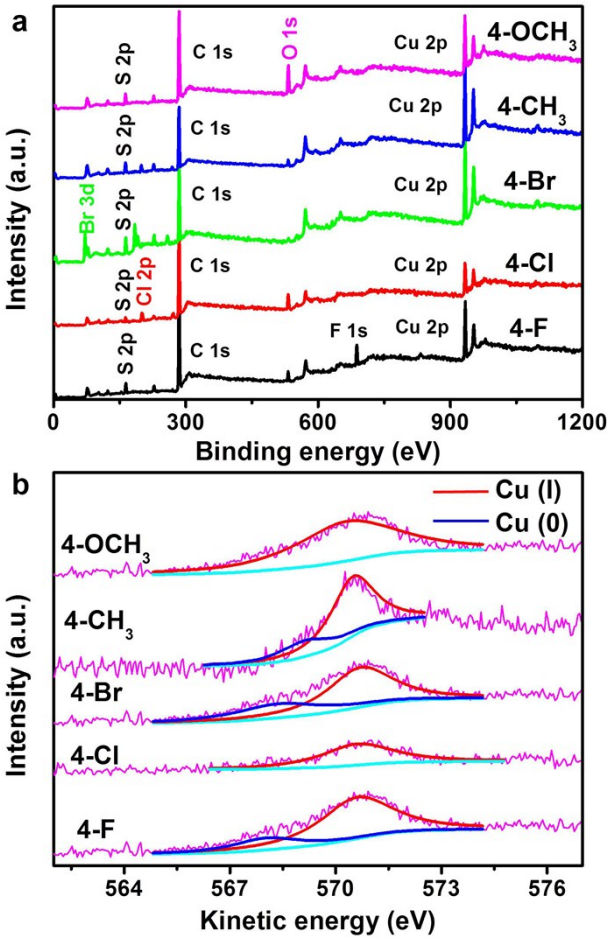

Figure S5. TGA curves (a-e) of the Cu NCs self-assembly architectures heated under N_2 atmosphere from room temperature to 900 ^oC. FTIR spectra (f-j) of the Cu NCs self-assembly architectures. The disappeared SH peak indicates the formation of Cu-S bond.

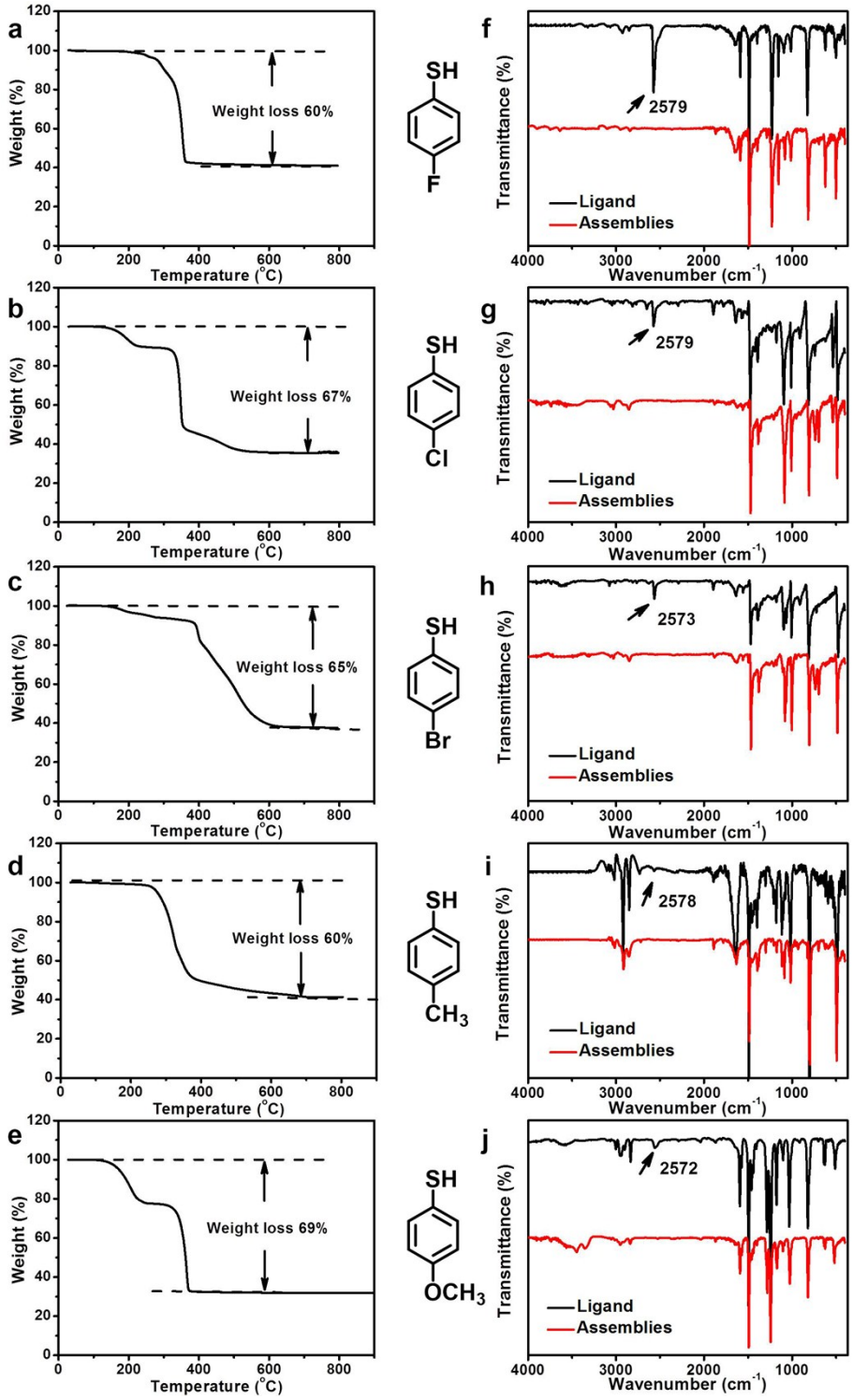

Figure S6. PL excitation spectra of the Cu NCs self-assembly ribbons capped with different para-substituted thiophenol.

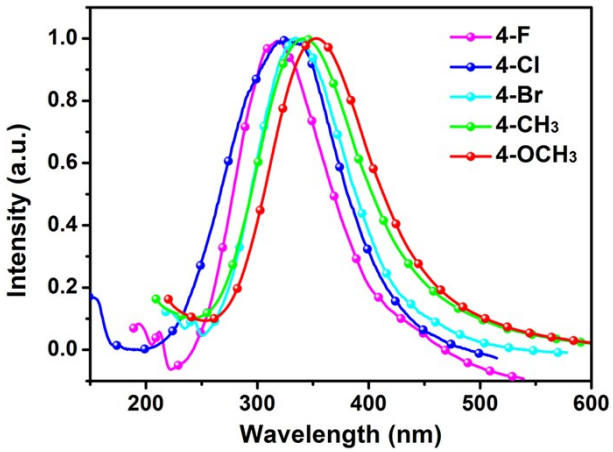

Table S1. Comparison of the peak positions of PL excitation (Ex) and emission (Em) spectra, PLQYs, and emission lifetimes of the Cu NCs self-assembly ribbons capped with different para-substituted thiophenol.

Substituent group	Ex (nm)	Em (nm)	PLQYs (%)	Lifetime (μs)
OCH_3	351	698	3.0	5.7
CH_3	340	677	4.1	4.0
Br	334	659	7.9	3.6
Cl	327	646	13.9	2.9
F	316	548	15.6	1.8

Figure S7. PL emission spectra of the self-assembly architectures composed of Cu NCs capped by 4-fluorothiophenol (a), 4-chlorothiophenol (b), 4-bromothiophenol (c), 4-methylbenzenethiol (d), and 4-methoxybenzenethiol (e) in chloroform as excited at 365, 380, 400, 420, and 440 nm. The emission is independent on the excitation wavelength. It means that the self-assembly architectures possess homogeneous chromophores, namely, the sole triplet state T1.

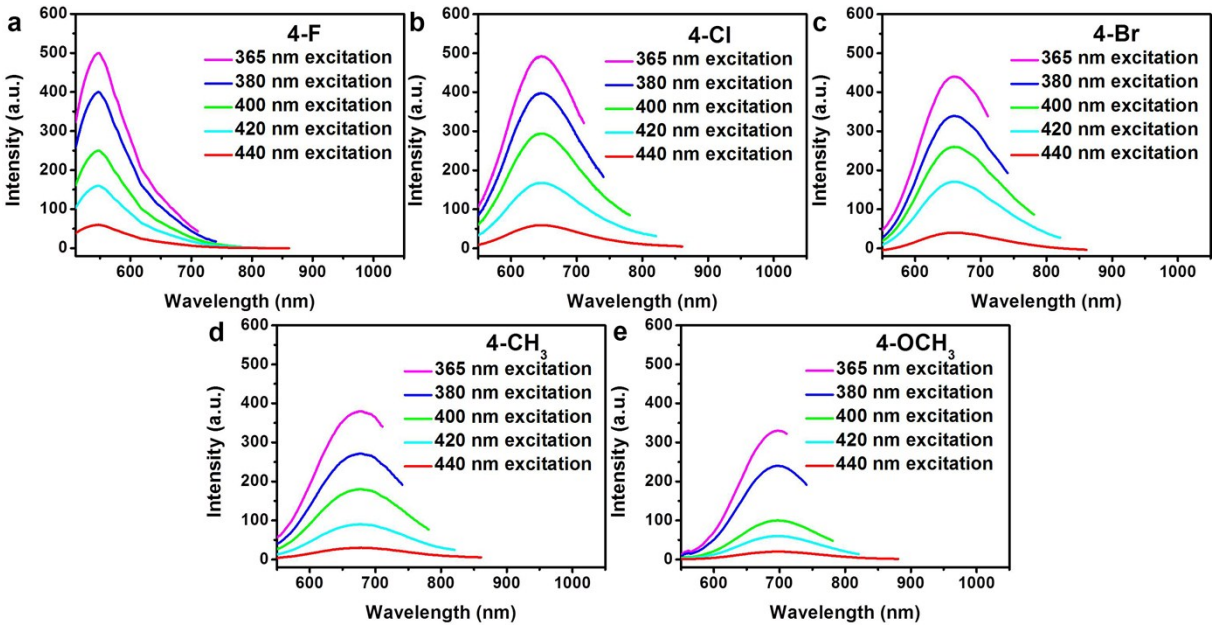

Figure S8. The variation of emission spectra (a-e) of Cu NCs self-assembly architectures with 365 nm excitation from 77 to 298 K. Room-temperature luminescence lifetimes (f-j) of Cu NCs self-assembly architectures with 400 nm excitation, which exhibit long excited-state lifetime of 1.8, 2.9, 3.6, 4.0, and 5.7 μs. The chemical structures of capping ligands are shown between temperature-dependent emission spectra and luminescence lifetime data. The luminescence lifetime fit parameters is fit = $B_1\exp(-t/\tau_1)+ B_2\exp(-t/\tau_2)$. $\tau_{ave} = \frac{\Sigma_i B_i \tau_i^2}{\Sigma_i B_i \tau}$.

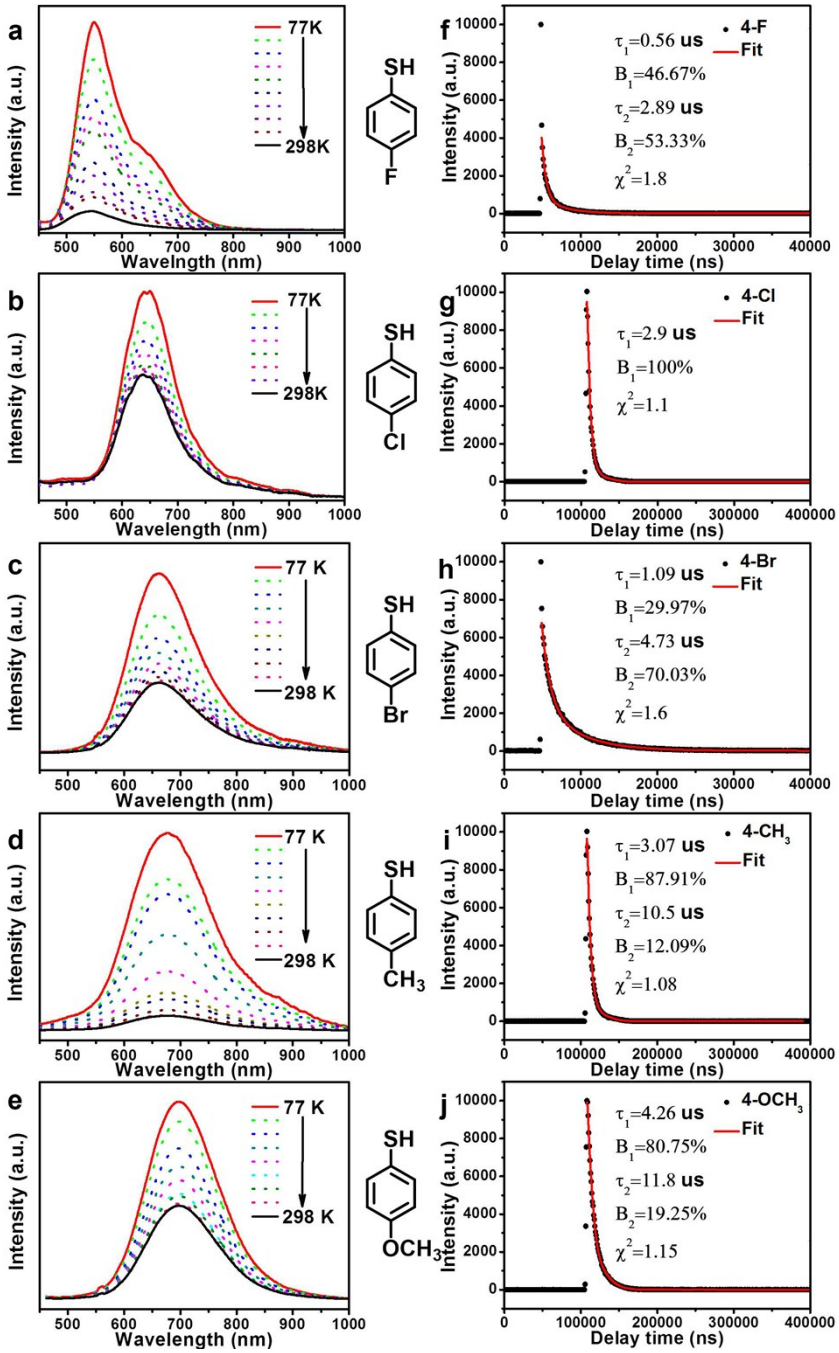

Figure S9. (a) Geometric structure and Kohn-Sham molecular orbitals (isosurface value 0.035 a.u.) of the NCs capping with different para-substituted thiophenols are shown from front view. (b) The optimized structures (from top view) and calculated vertical absorption energies of the corresponding five NCs shown in Figure a. Copper atoms are shown in orange, sulfur in yellow, carbon in gray, hydrogen in white, fluorine in blue, chlorine in green, bromine in violet, and oxygen in red. L represents for the capping ligands.

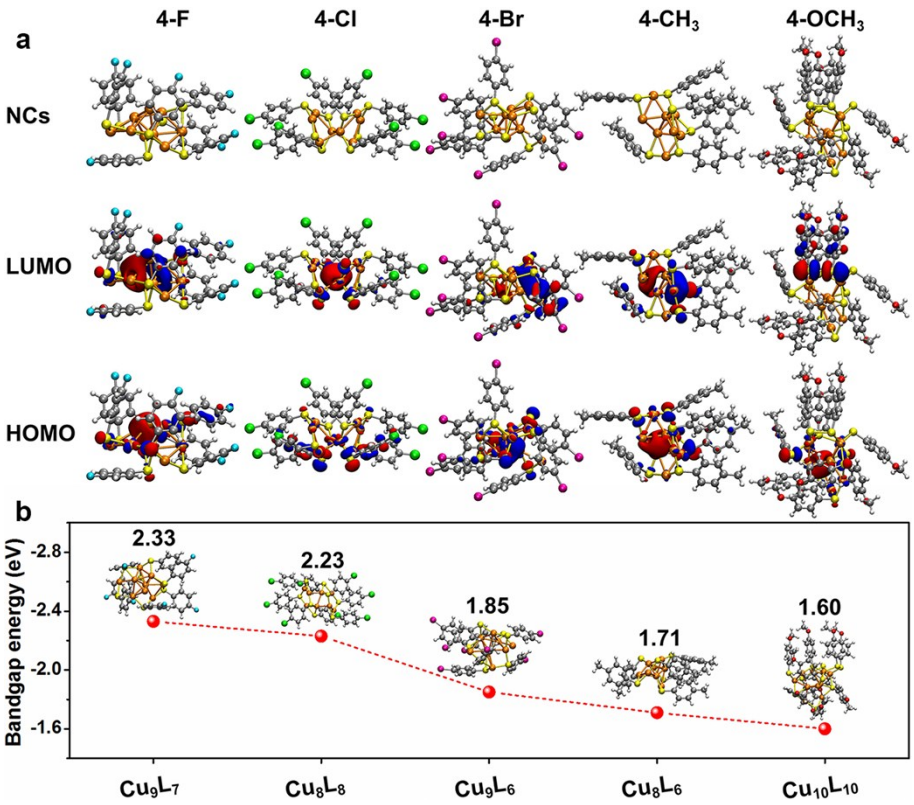

Figure S10. (a) XRD patterns of Cu NCs self-assembly architectures. With the increase of ligands electron-donating ability, the intensity of XRD peaks decreases. (b) Summaries of the full-width at half-maximum of XRD first diffraction peak (red line), which gradually broadens from F to OCH_3 substituted products, and the intensity of XRD first diffraction peak (blue line), which gradually decreases from -F to -OCH_3 substituted products.

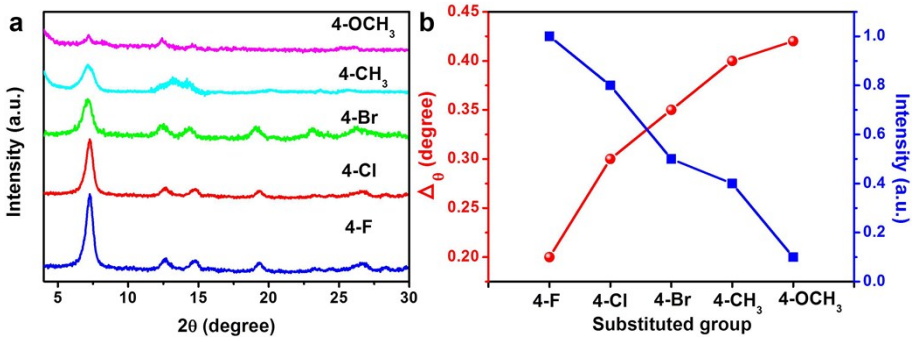

Figure S11. MALDI-TOF mass spectra of Cu NCs self-assembly architectures. MALDI-TOF mass spectra exhibit the composition of $Cu_8(2\text{-}Cl)_8$ (a), $Cu_8(3\text{-}Cl)_8$ (b), $Cu_8(4\text{-}Cl)_8$ (c), and $Cu_7(3,\ 5\text{-}2Cl)_7$ (d), respectively. L represents for the capping ligands in MALDI-TOF analysis peaks. Insets are corresponding chemical structures of the capping ligands.

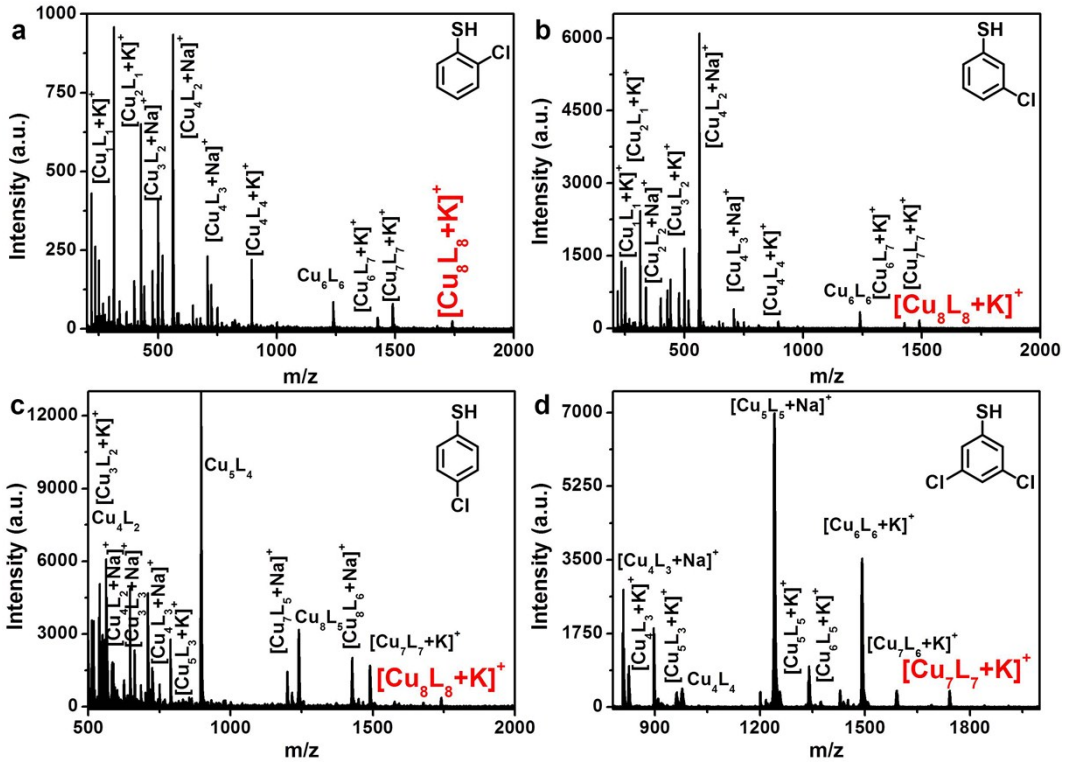

Figure S12. Schematic electronegative resonance structures of 2-chlorothiophenol, 3-chlorothiophenol, and 4-chlorothiophenol.

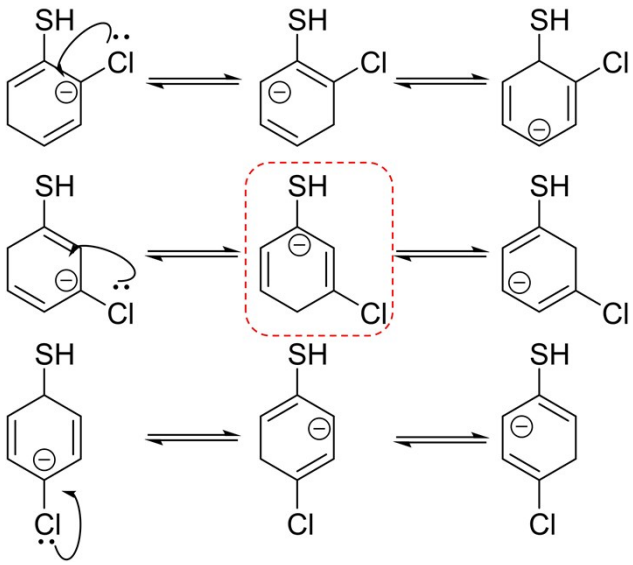

Table S2. Comparison of the PL peak positions and QYs of the Cu NCs self-assembly architectures capping with 2-chlorothiophenol, 3-chlorothiophenol, 4-chlorothiophenol, and 3,5-dichlorothiophenol, respectively.

Substitution site	PL (nm)	PLQYs (%)
2-Cl	647	1.3
3-Cl	681	2.4
4-Cl	646	13.9
3,5-2Cl	695	2.0

Figure S13. Low (a-e) and high (f-j) magnification TEM images of Cu NCs self-assembly architectures from the copper sources of $CuCl_2$ (a, f), $CuAc_2$ (b, g), $CuSO_4$ (c, h), $Cu(acac)_2$ (d, i), and $Cu(NO_3)_2$ (e, j). High magnification TEM images indicate that the self-assembly architectures are composed of ultrasmall NCs, denoted by red circles. Steady-state absorption (k) and PL emission spectra (l) of the self-assembly architectures from different copper sources.

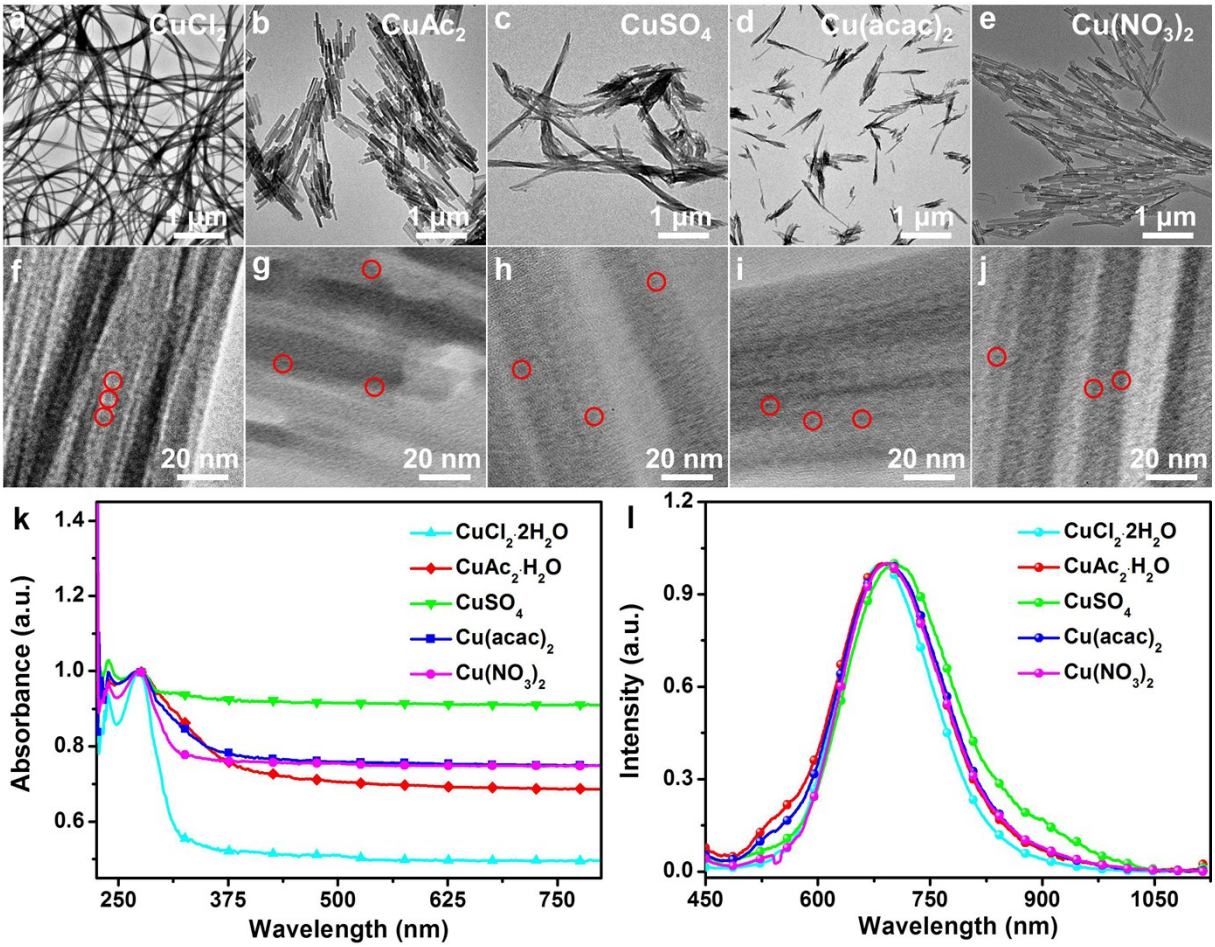

Figure S14. (a) The fluorescent intensity of Cu NCs self-assembly architectures capped by 4-chlorothiophenol *versus* the storage duration. After one year, the QY is still over 13.0%. (b) Comparison of the PL emission spectra of solid powder of the self-assembly architectures composed of Cu NCs capped by 4-chlorothiophenol before and after grind.

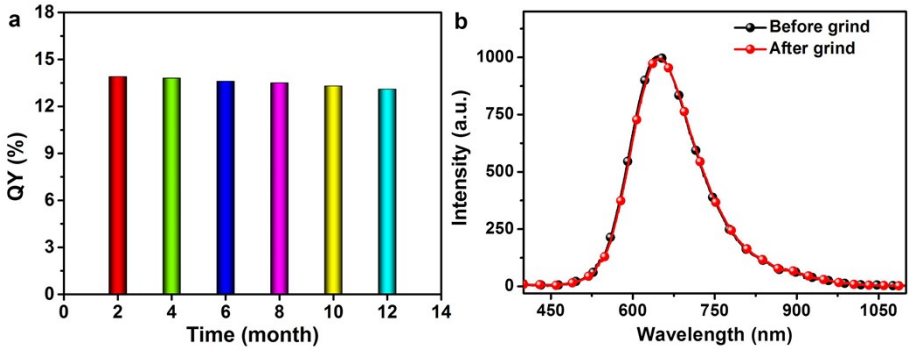

Figure S15. The electroluminescent spectrum of GaN LED chip. The emission centers at 365 nm.

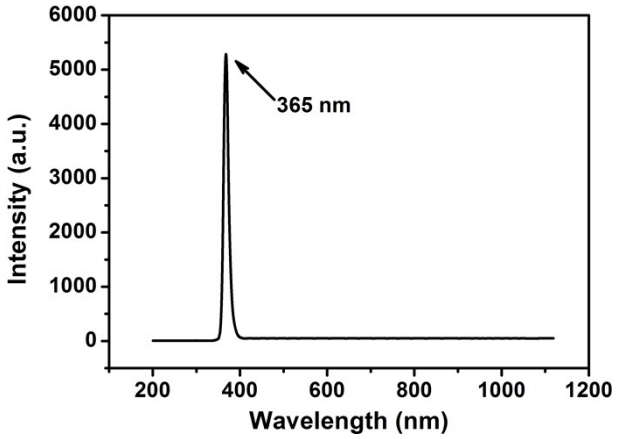

Figure S16. The emission spectrum of sunlight.